crystals

MDPI

Article

Study on the Microstructure and Wear Properties of Al_2O_3-3%TiO_2-xAl Composite Coatings Prepared by Plasma Spraying

Pengyu Dai [1], Yu Zhang [1,*], Xin Wang [1], Jiahang Yan [1], Lin Zhao [2,*] and Xiaohong Yi [3,*]

[1] School of Mechanical Engineering, Shenyang University, Shenyang 110044, China
[2] Institute of Metal Research, Chinese Academy of Sciences, Shenyang 110016, China
[3] Research Institute of Tsinghua, Pearl River Delta, Guangzhou 528000, China
* Correspondence: nihao9985@163.com (Y.Z.); zhaolin@imr.ac.cn (L.Z.); yixhong@163.com (X.Y.)

Abstract

Al_2O_3-3% TiO_2-xAl (x = 0, 20, 40, 60 wt.%) composite coatings were prepared on Q235 substrate by plasma spraying technology, and the effects of pure Al phase addition on the microstructure and wear properties of the coatings were compared and analyzed. The results show that a unique splash-like structure was formed on the surface of the coating, and this structure became more obvious with the increase in Al content. Cross-sectional analysis shows that the introduction of pure Al phase reduces the large pores and cracks in the coating, forming a slender band structure. XRD analysis shows that the addition of pure Al phase leads to a decrease in the diffraction peak intensity of α-Al_2O_3, while the diffraction peak intensity of Al phase and γ-Al_2O_3 gradually increases, especially in the coating with 40% Al content; the diffraction peak of γ-Al_2O_3 increases significantly. XPS analysis further confirms that with the increase in Al content, a new pure Al peak appears in the Al element spectrum, and the peaks of α-Al_2O_3 and γ-Al_2O_3 fluctuate. In addition, the porosity of the coating decreases first and then increases and then decreases again with the increase in Al content. The porosity of the coating with 60% Al content is the lowest, at only 5.14%. Microhardness test results show that with the increase in Al content, the microhardness of the coating gradually decreases, and the fracture morphology changes from brittle fracture to irregular fracture, with the appearance of pull-out areas, indicating that the pure Al phase effectively improves the brittleness of the coating. However, the friction and wear test results show that the friction coefficient of the coating increases with the increase in Al content. The pure Al_2O_3 coating has high hardness and excellent wear resistance, while the coating with 60% Al content has the highest friction coefficient and the most severe wear. Moreover, adhesive wear phenomena appear on the coating surface with high Al content.

Keywords: plasma spraying; ceramic coatings; pure Al phase; microstructure

check for updates

Academic Editor: Vladislav V. Kharton

Received: 25 August 2025
Revised: 7 September 2025
Accepted: 9 September 2025
Published: 15 September 2025

Citation: Dai, P.; Zhang, Y.; Wang, X.; Yan, J.; Zhao, L.; Yi, X. Study on the Microstructure and Wear Properties of Al_2O_3-3%TiO_2-xAl Composite Coatings Prepared by Plasma Spraying. *Crystals* **2025**, *15*, 809. https://doi.org/10.3390/cryst15090809

Correction Statement: This article has been republished with a minor change. The change does not affect the scientific content of the article and further details are available within the backmatter of the website version of this article.

Copyright: © 2025 by the authors. Licensee MDPI, Basel, Switzerland. This article is an open access article distributed under the terms and conditions of the Creative Commons Attribution (CC BY) license (https://creativecommons.org/licenses/by/4.0/).

1. Introduction

With the advancement of industrial technology, optimizing the surface properties of metal materials has remained a crucial research focus, particularly in enhancing material hardness, wear resistance, and corrosion resistance through surface treatment methods. Plasma spraying technology, as an advanced surface treatment technique, holds significant importance in industrial applications [1]. This method utilizes high-temperature plasma arc flame streams to melt coating materials, which are then ejected onto substrate surfaces

under high-speed airflow to form specialized coatings. Due to its efficiency, process stability, and broad material applicability, plasma spraying has been widely adopted in aerospace, automotive manufacturing, and energy chemical industries. It can produce various coatings including metal coatings, metal-ceramic coatings, and ceramic coatings [2–4], with Al_2O_3-based coatings demonstrating exceptional corrosion resistance and wear durability, making them extensively used. However, the poor fluidity of molten droplets during Al_2O_3 preparation leads to surface defects such as microcracks, pores, and streaks that significantly impact coating performance. The classic composite ceramic coating Al_2O_3-3% TiO_2 (AT3) [5] reduces alumina melting point and porosity through TiO_2 addition. The formation of minor intermetallic compounds during AT3 preparation also improves coating properties. Nevertheless, AT3 coatings exhibit low toughness and high brittleness, making them prone to damage and limiting their application in high-strength, high-impact environments.

To overcome these limitations, researchers have attempted to introduce metal phases into Al_2O_3-coated materials to optimize their performance. Zhu, H.Q. et al. [6] developed Cu-Ni-Al_2O_3 composite coatings with varying Ni content on AZ91D magnesium alloy substrates using low-pressure cold spray technology. Their analysis of microstructure, morphology, and mechanical properties demonstrated that controlled Ni content effectively reduced porosity while enhancing deposition efficiency, bonding strength, and wear resistance. Liu, X.Y. et al. [7] created Ni-Zn-Al_2O_3 composite coatings with different zinc concentrations through the same method. The Zn powder content initially reduced pore size before increasing it, with optimal mechanical properties achieved at 14% zinc mass fraction. Sun, Y.H. et al. [8] implemented laser cladding to produce high-hardness, corrosion-resistant Ni-x%Al_2O_3 composites on 304 stainless steel. Their study revealed that Al_2O_3 content significantly influenced coating morphology, microhardness, and corrosion resistance. The composite formed a tight metallurgical bond with the substrate, exhibiting microstructures progressing from surface to core: equiaxed grains, oriented columnar crystals, and acicular crystals. Notably, microhardness increased initially but decreased with higher Al_2O_3 content, while weight-dependent corrosion rate first decreased then increased, corrosion potential rose initially but later declined, and current density decreased initially before rebounding.

Experimental studies by the aforementioned scholars demonstrate that adding metallic phases can enhance the plastic deformation capability of ceramic coatings. These metallic phases not only fill pores in the coating to improve density but also strengthen the coating's toughness and bonding strength with the substrate. Among various effective metallic phase additives, aluminum (Al) stands out as an ideal choice for metal-ceramic composite coatings due to its lightweight and active properties, which provide excellent plastic deformation capacity and oxidation resistance. Wang, Q.Q. et al. [9] developed Al-Al_2O_3 composite coatings with varying aluminum content using atmospheric plasma spraying technology, systematically investigating the effects of aluminum content on coating microstructure, mechanical properties, wear resistance, and corrosion resistance. Results showed that increasing aluminum content from 5% to 30% gradually reduced coating hardness while enhancing fracture toughness. Wear resistance initially improved but later declined, whereas corrosion resistance first increased and then decreased with higher aluminum content. Wang, C.H. et al. [10] fabricated Al/Al_2O_3 composite coatings via flame spraying, revealing that pore volume increased with Al_2O_3 powder content. The coating with 15% Al_2O_3 mass fraction exhibited the lowest porosity, while polarization curves indicated that coatings with 20% Al_2O_3 mass fraction demonstrated optimal corrosion resistance. These findings are consistent with previous studies on metal-ceramic coatings, such as Ren et al. [11], who also observed similar microstructural improvements in Al-Al_2O_3

coatings prepared by supersonic plasma spraying. However, our study further elucidates the role of Al content in mediating the transition from brittle to ductile fracture modes. Their study investigated the effects of Al_2O_3 particle loading on microstructure, porosity, electrochemical performance, and salt spray corrosion resistance. The results revealed wavy surface patterns with tightly bonded internal structures. The 70% Al_2O_3 coating exhibited the highest porosity (6.71%), while 70% Al_2O_3 coatings showed minimal corrosion and demonstrated optimal anti-corrosion properties. Wang, K. [12] and collaborators created high-performance 7075Al/Al_2O_3 composite layers by incorporating large-sized Al_2O_3 spherical particles into 7075Al powder. Their research demonstrated that increased Al_2O_3 particle content enhanced plastic deformation during cold spraying, improved interparticle bonding, and reduced pore formation defects.

In summary, the introduction of pure Al phases can modify the microstructure, hardness, and wear resistance of ceramic coatings, thereby enhancing their overall performance. This has a positive impact on the application scope of Al_2O_3 ceramic coatings. However, previous studies have paid insufficient attention to how the incorporation of pure Al phases affects the microstructure of coatings and the formation mechanisms between coatings. To address this gap, this paper employs plasma spraying technology to fabricate Al_2O_3-3%TiO_2-xAl (x = 0, 20, 40, 60 wt.%) composite coatings on Q235 base materials. The study focuses on analyzing the effects of pure Al phase incorporation on the microstructure and fundamental properties of the coatings, providing theoretical foundations and technical support for optimizing the performance of plasma-sprayed coatings.

2. Materials and Methods

2.1. Experimental Materials

The substrate used in this spray coating experiment is Q235 steel. Wire cutting was employed to cut the substrate into two test specimens of different sizes (20 mm × 20 mm × 4 mm) for later use. Post-cutting, the coating surface retained rust and oil residues that required further treatment. An air compressor was used to compress gas before spraying, ensuring the gas pressure reached 0.6~0.8 Mpa [13,14]. The substrate was then sprayed using a sandblasting machine. Impurities and rust on the surface were removed through impact with 80-mesh white corundum sand, transforming the smooth surface into a textured matte finish to enhance coating adhesion. The powder used in the experiment contains 0%, 20%, 40%, and 60% aluminum content in Al_2O_3-3% TiO_2-xAl mixed powder produced by China Metallurgical Xindun Alloy Co., Ltd. Xingtai City, Hebei Province. All powders are spherical with diameters ranging from 15 to 50 μm. Prior to spraying, the powder underwent over 12 h of drying in a 50 °C drying chamber for heating.

2.2. Experimental Method and Process

This experiment employed the SX-80 plasma spraying equipment manufactured by Guangzhou Sanxin Technology Co., Ltd. Guangzhou, Guangdong Province, China. for the coating process, with the following parameters, as shown in Table 1. The substrate was cut into two sizes of test pieces using wire cutting for subsequent use, with the experimental test piece size being 20 mm × 20 mm × 4 mm. The cut coating surface may retain rust stains and oil residues, requiring further treatment. A Utheisa Kong air compressor by Guangzhou Jiangcheng Compressor Co., Ltd. Guangzhou, Guangdong Province was used to compress the gas before ejection, ensuring the ejected gas pressure ranged between 0.6~0.8 MPa. The substrate was then sandblasted using a sandblasting machine. Under the impact of 80-mesh white corundum sand, impurities and rust stains on the substrate surface were removed, transforming the smooth surface into a rough, matte texture to facilitate better contact between the coating and the substrate. The main gas argon is at

0.7 MPa, the secondary gas hydrogen is at 0.4 MPa, and the cooling water pressure is at 1.7 MPa. Spraying current 380 A, 480 A and 580 A. The spraying voltage is 27 V. To address the common nozzle clogging issue during high-aluminum coating preparation, the power output was reduced to ensure smooth material deposition.

Table 1. The corresponding parameters and process parameters of coatings with different Al contents.

Voltage (V)	Current (A)	Dusty Spray	Painting Distance (mm)	Argon Pressure (Mpa)	Argon Gas Flow ($kg \cdot cm^{-2}$)	Feed Flow Rate ($L \cdot h^{-1}$)	Firing Voltage (V)
27	580	AT3-0% Al	100	0.7	100	300	3
27	480	AT3-20% Al AT3-40% Al	100	0.7	100	300	3
27	380	AT3-60% Al	100	0.7	100	300	3

The coating was examined using an S-4800 II scanning electron microscope by Suzhou Sainz Instrument Co., Ltd. Suzhou City, Jiangsu Province equipped with an EDS for morphological observation and elemental analysis. Surface images at the same magnification obtained from the scanning electron microscope were processed through Image-J software (1.53t) to measure porosity and analyze pore distribution. Images were converted to 8-bit grayscale. A threshold value was set to distinguish pores from the matrix (typically between 0 and 50 on a 0–255 scale). The "Analyze Particles" function was used with a circularity range of 0.3–1.0 to exclude non-pore artifacts. The coating was sectioned using a metallographic experimental cutting machine, followed by sample embedding, grinding, and polishing. Post-treatment coating sections were tested with a HXD-1000 digital microhardness tester manufactured by Shanghai Taoming Optics Co., Ltd. Shanghai, China, employing 1000 g loading force for 15 s. A HXD-1000 microhardness tester was used with a Vickers indenter. A load of 1000 gf was applied for 15 s. Ten measurements were taken for each sample at different locations to avoid overlap. The instrument was calibrated using a standard hardness block before each session. The average value and standard deviation are reported. Friction wear performance of Al-containing AT3 coatings produced by plasma spraying was evaluated using an HT-500 friction wear tester by Jinan Chengyu Experimental Equipment Co., Ltd., Jinan, China. Specimens measuring 20 mm × 20 mm × 10 mm were plasma-coated, with 1500 HV silicon nitride (density: 3.2~3.3 g/cm^3) serving as the abrasive ball. The lightweight silicon nitride reduced inertial loads on moving parts. Test parameters included 10 N load, 30 min duration, and 500 rpm motor speed. The abrasive balls were controlled to maintain a 5 mm distance from the sample center, creating a 10 mm circular scratch. Impact tests were conducted using a pointer impact tester by Jinan Times Assay Instrument Co., Ltd., Jinan, China to observe fracture modes of coatings with varying aluminum content.

3. Experimental Results and Analysis

3.1. Surface Morphology Analysis of Coating

Figure 1 shows the surface microstructure of the AT3-X% Al coating. The macroscopic morphology exhibits characteristic lamellar distribution patterns, which are formed when powder particles are heated to a molten state during plasma spraying and rapidly solidify upon impact with the substrate surface under high-speed airflow [15]. Macroscopic observation reveals a coexistence of fully melted zones and partially fused regions in the coating, a phenomenon closely related to powder particle size, nozzle power parameters, and spatial distribution of powders within the spray gas flow.

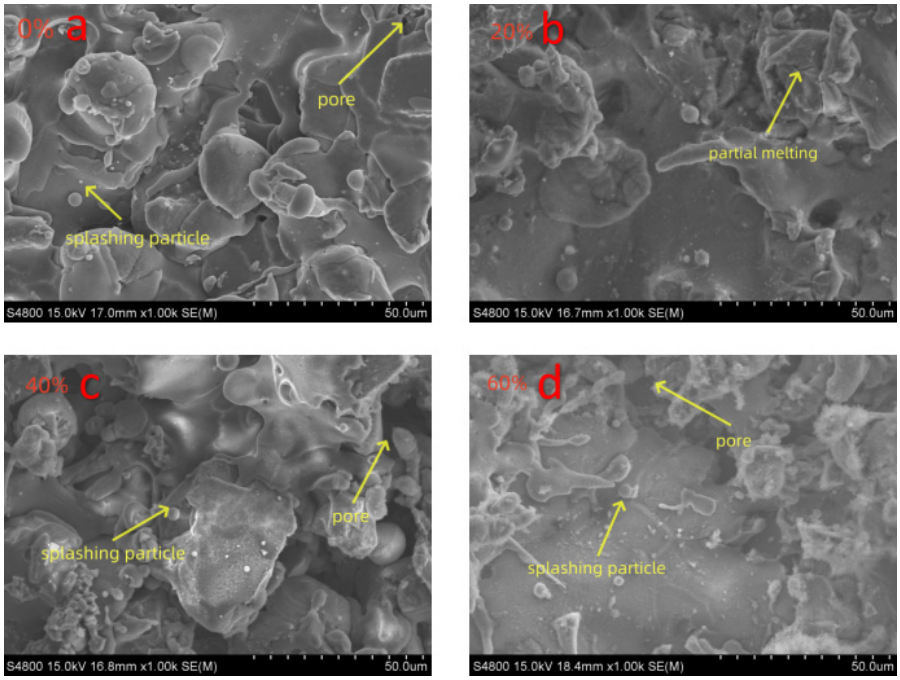

Figure 1. SEM morphology of coating surfaces with different Al content ×500. (**a**) 0%, (**b**) 20%, (**c**) 40%, (**d**) 60%.

Figure 1a shows the surface morphology of the AT3 coating. The coating exhibits numerous granular aggregates, representing typical partially fused zones with higher porosity. During plasma spraying, when molten alumina particles contact the substrate surface and rapidly cool, the resulting thin and brittle cooling layer is prone to cracking and spatter. This spatter pattern is commonly observed in high-melting-point materials such as metal oxides and alloys.

Figure 1b–d shows the morphology of the coating after increasing the Al content. When a part of Al is added to the coating, the partial melting zone is significantly reduced. At this time, during the spraying process, the melting point of the sprayed powder is significantly reduced, forming Al-coated AT3 molten droplets.

During the coating formation process, the observed sputtering morphology primarily results from the cooling of larger droplets. When molten droplets are subjected to the spray gun's airflow on the substrate surface, they transition from spherical to flattened or oval shapes. When the applied force exceeds the surface tension of the droplet, it breaks into smaller droplets. This sputtering pattern predominantly occurs in low-melting-point soft materials such as aluminum (Al) and chromium (Cr). Notably, as the aluminum content increases, both the particle size and quantity of sputtered particles shown in Figure 1 show significant reduction.

The introduction of pure Al phases significantly alters the microstructure of the coating, exhibiting a bimodal distribution characterized by both classical flake-like and sputtered structures. Concurrently, as Al content increases, the coating surface color transitions from gray-black to gray-white. These structural features and color changes primarily result from differences in surface tension and solidification rates between molten Al_2O_3 and Al, which create distinct microstructures under spray gun airflow. Additionally, insufficient melt contraction during solidification generates localized tensile stress between particles. When this tensile stress exceeds the material's fracture strength, microcrack defects form within the coating. This phenomenon is particularly pronounced in aluminum-based coatings, where the incorporation of pure Al phases substantially reduces the likelihood of crack formation.

Figure 2 shows the SEM image of the coating surface and elemental distribution patterns. The plasma spray-coated layer exhibits an uneven surface due to airflow impact, sputtering, and molten droplet spreading. During EDS electron bombardment, charge accumulation in depressions hinders electron escape, resulting in weak secondary electron signals that obscure elemental analysis [16]. Consequently, the elemental distribution maps display completely black areas primarily located in depressions, which are not impurities but rather material components.

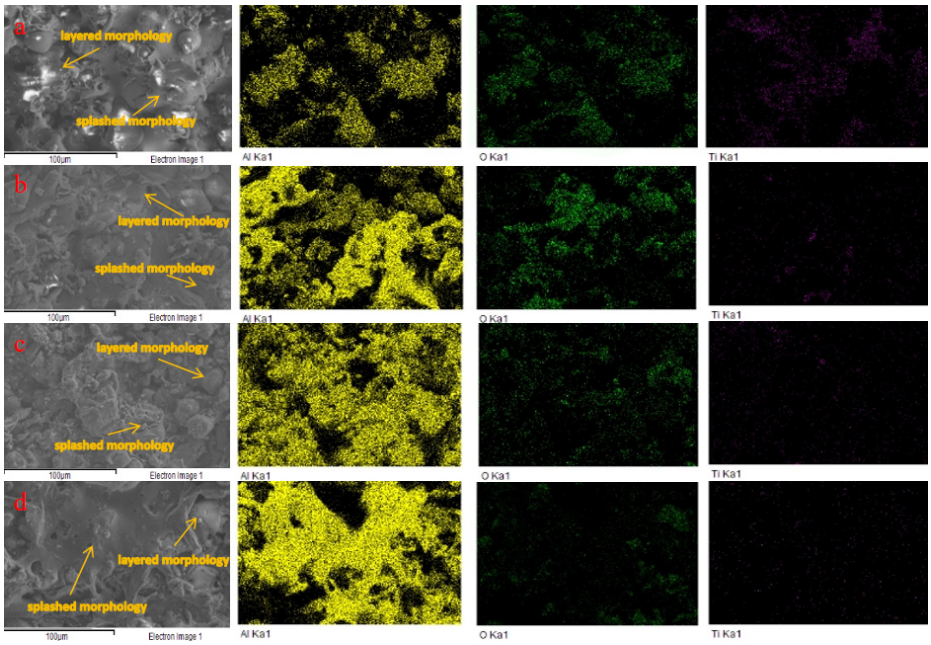

Figure 2. Elemental distribution of coating surfaces with different Al contents. (**a**): SEM image with 0% aluminum content. (**b**): SEM image with 20% aluminum content. (**c**): SEM image with 40% aluminum content. (**d**): SEM image with 60% aluminum content.

As the Al content in the spray powder is gradually added, the proportion of Al elements in the coating increases while the O content decreases. SEM image analysis reveals that the surface layers predominantly consist of Al_2O_3 phases, whereas the wavy patterns mainly form pure Al structures. This phenomenon arises from the differing melting points and solidification shrinkage rates of Al and Al_2O_3. During spraying, under airflow action, Al particles disperse before solidification, resulting in wavy patterns. In the formation of AT coatings, titanium elements coexist with oxygen but concentrate in coating defects such as pores and sputtered particle edges. With increasing Al content in the coating, titanium content decreases progressively, thereby reducing its impact on coating performance.

3.2. Cross-Sectional Morphology Analysis of Coating

Figure 3 presents the cross-sectional image and elemental distribution of the AT3-X% Al coating. The results demonstrate that coatings with varying aluminum content all exhibit the characteristic lamellar structure typical of thermal spray coatings. Under identical spraying conditions, the coating thickness decreases as aluminum content increases, which stems from two primary mechanisms: First, higher aluminum content causes excessive heating of powder at the spray gun's feeding nozzle, leading to reduced fluidity and decreased powder feed rate. Second, when aluminum content exceeds 40% in the powder, rapid agglomeration and coagulation of aluminum particles occurs within the spray gun's

molten arc. These aggregated particles form solidified chunks before reaching the substrate, resulting in detachment from the spray gun beam and ultimately thinning the coating.

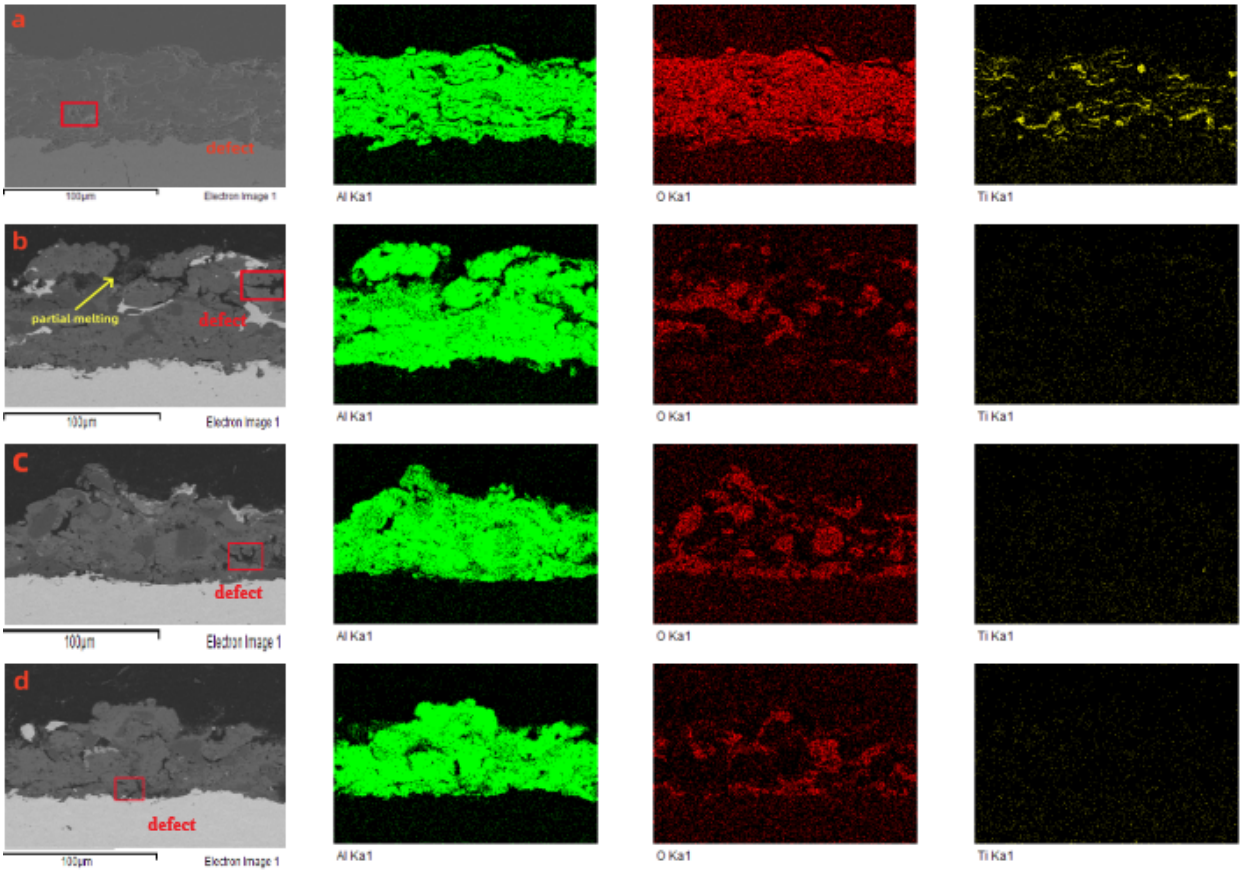

Figure 3. Elemental distribution of cross-sections of coatings with different Al contents (**a**): AT3-0% Al (**b**): AT3-20% Al (**c**): AT3-40% Al (**d**): AT3-60% Al.

When pure aluminum phase is incorporated into the coating, the layered structure undergoes subtle transformations. The original elongated strip-like morphology becomes slender and elongated, with a marked reduction in pores and defects in the underlying coating. This occurs because during the coating preparation process, molten Al_2O_3 droplets contact the cooler substrate, rapidly solidifying an outer cooling layer while maintaining a semi-solid or softened interior. Subsequent droplet impacts cause plastic deformation in the partially cooled interior, forming elongated strip-like lamellar structures. The addition of pure aluminum phase results in a lower layer with slender elongated strips and an upper layer exhibiting thickened lamellar morphology. The lower layer demonstrates optimized coating performance and reduced defects due to the pure aluminum phase. Meanwhile, the upper layer achieves a naturally spherical structure through spontaneous slow cooling after the spraying process, free from subsequent particle bombardment or pressure effects.

The elemental distribution analysis indicates that as Al content increases, green bright regions (Al elements) become more abundant and uniformly distributed, while internal black voids (defects like pores and cavities) gradually diminish with fewer cracks appearing. Simultaneously, red areas (O elements) disintegrate into smaller regions, which correlates with reduced Al_2O_3 content. The reduction in coating defects after increased Al content stems from two mechanisms: During spraying, high-temperature spray guns melt powder into molten droplets, forming Al-coated Al_2O_3 droplets. Since molten Al exhibits superior fluidity and thermal conductivity compared to Al_2O_3, these droplets deposit into more homogeneous structures. Additionally, slight oxidation between molten droplets

and ambient oxygen improves elemental distribution uniformity while reducing coating defects. Yellow areas (Ti elements) exhibit band-like distributions at coating striations and pores, positively contributing to lowering the porosity of AT3 coatings. However, with increased Al content, defects in the coating significantly decrease, while Ti element proportions diminish markedly, predominantly appearing as dot-like dispersion across different coating regions.

3.3. XRD Analysis of Coating

Figure 4 shows the XRD patterns of AT3 composite coatings with Al content levels of 0%, 20%, 40%, and 60%. The XRD analysis reveals distinct differences between the pure AT3 curve and the three Al-containing curves. As pure Al phases are introduced, the number of peaks significantly decreases, the curves become smoother, and the intensity of the main peak markedly diminishes. The three Al-containing curves exhibit nearly identical peak positions and intensities, each displaying three strong diffraction peaks at 38.6°, 44.8°, and 65.2° corresponding to the pure Al phase. The primary phases consist of pure Al and α-Al_2O_3 phases, with minor amounts of TiO_2 and γ-Al_2O_3 phases present.

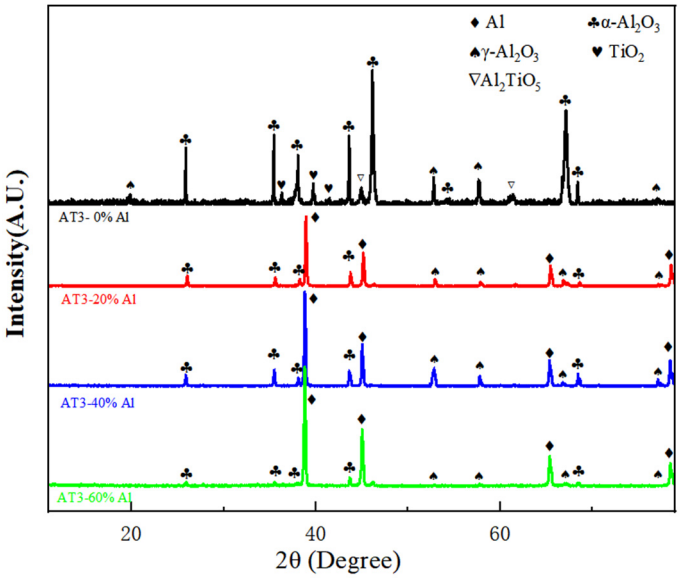

Figure 4. XRD patterns of coatings with different Al contents.

The XRD pattern reveals two characteristic peaks in the coating: α-Al_2O_3 (stable state) and γ-Al_2O_3 (unstable state). The stable α-Al_2O_3 originates from the original powder, determined by its grain boundary structure. This structure features oxygen ions arranged in a close-packed hexagonal lattice, with aluminum atoms filling the octahedral voids, resulting in a high melting point that resists melting [17].

When spraying high-alumina powder, reduced spraying power causes changes in the spray gun's central temperature. The lowered flame temperature becomes insufficient to complete the conversion from γ-Al_2O_3 to α-Al_2O_3 phases. This results in noticeable γ-Al_2O_3 phase formation within the coating after adding pure aluminum phase. Additionally, the excellent thermal conductivity of pure aluminum enables rapid temperature reduction. The molten α-Al_2O_3 phase contacts the cooler aluminum or substrate, leading to accelerated cooling and non-equilibrium solid-state transformation that generates γ-Al_2O_3 phase. Due to its lower critical free energy, γ-Al_2O_3 undergoes faster nucleation during spraying [18,19], resulting in partial γ-Al_2O_3 phase formation in the coating. Al_2TiO_5 phase appears in pure AT3 coatings. As the aluminum content increases, the intensity of Al_2TiO_5 diffraction peaks decreases significantly, which correlates with reduced TiO_2 content in the powder.

3.4. Analysis of Friction and Wear Behavior of AT3 Coatings with Different Al Contents

Figure 5 shows the friction coefficient versus time curves of coatings with varying aluminum content under a 10 N load. The results indicate that the pure AT3 coating exhibits the lowest friction coefficient, which initially rises from 0 to 260 s before stabilizing without significant fluctuations. Coatings containing 20% and 40% aluminum show comparable friction coefficients, but the 40% aluminum coating demonstrates dramatic fluctuations throughout the experiment, failing to reach a stable state until completion. In contrast, the 20% aluminum coating maintains a relatively smooth trajectory. The 60% aluminum coating exhibits an initial rise followed by a decline, attributed to aluminum agglomeration that creates uneven surface irregularities. These high-aluminum regions exhibit poor wear resistance, resulting in higher friction coefficients. When these protrusions are worn away, the coating becomes smoother and the coefficient decreases, explaining the observed rise-and-fall pattern. As pure aluminum content increases, the friction coefficient rises significantly, with the 60% aluminum coating reaching a peak of 0.659 while the AT3 coating remains the lowest at 0.418.

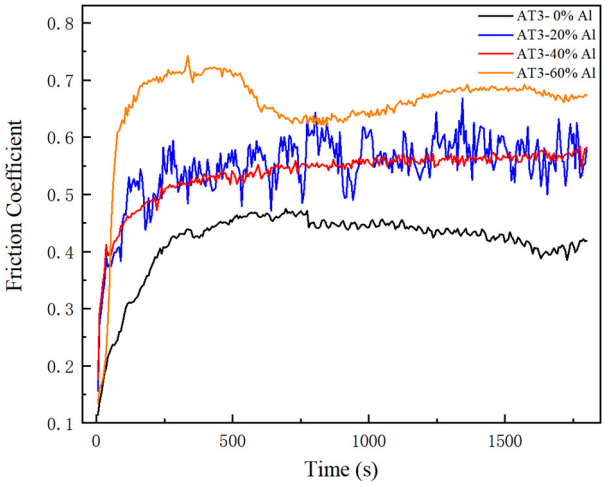

Figure 5. Curve of friction coefficient versus time for coatings with different Al content at 10 N load.

By analyzing the results in Figures 5 and 6 alongside the friction coefficient curves, it is evident that the pure AT3 coating, due to its high material hardness and superior wear resistance, showed no surface scratches. The coating only exhibited flake-like surface wear forming bright areas. As the proportion of pure Al phase increased, surface abrasions became more pronounced with widened grooves. While scratch edges developed partial convex patterns, fewer holes appeared at these marks, fewer strip-shaped plow grooves remained, and the coating base gradually became smoother. The 60% Al content coating demonstrated particularly neat grooves with minimal convexity. Notably, adhesive wear was observed on 60% Al scratches, where removed pure Al particles adhered to the grinding balls and migrated with mechanical movement. In contrast, 20% and 40% Al coatings exhibited uneven surface irregularities. The visible scratches on the coating surface indicate significantly reduced wear resistance from added Al phases, consistent with observed changes in hardness and friction coefficients. The groove-like surface features with distinct undulations originate from incompletely melted particles or excessive agglomerates (Al_2O_3 particles) during spray deposition. These hard, poorly fused components detach from the coating surface under grinding ball pressure, creating characteristic grooves.

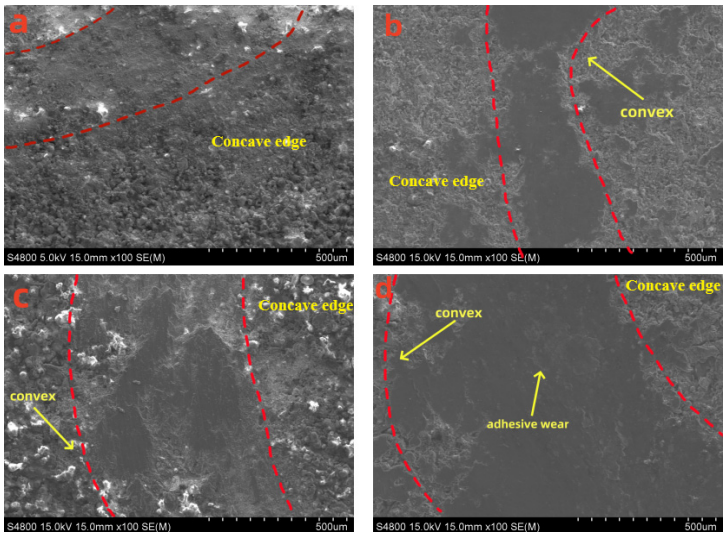

Figure 6. Scratch morphology of coatings with different Al contents (**a**): AT3-0% Al (**b**): AT3-20% Al (**c**): AT3-40% Al (**d**): AT3-60% Al.

Generally, Al_2O_3 has high inherent hardness. When pure aluminum is added to the coating, the overall hardness of the coating significantly decreases, and its friction coefficient also drops accordingly [20,21]. However, experimental results show that the friction coefficients of coatings containing 20% aluminum are comparable to those with 40% aluminum, and the surface wear morphology remains relatively similar.

Figure 7 isScratch edge morphology of coatings with different aluminum contents. The performance differences in coatings with varying aluminum content in sliding friction tests are closely related to their composition, phase structure, and defects. Coatings with 20% aluminum content contain more Al_2O_3 particles, exhibiting high hardness, excellent wear resistance, low friction coefficients, and stable fluctuations. During friction, Al_2O_3 particles may emerge or be driven out, causing surface cavities and irregularities. In 40% aluminum-content coatings, the ratio of pure aluminum phase to Al_2O_3 is approximately 1:1, with both phases diffusely distributed. During wear, alternating contact between the soft pure aluminum phase and hard Al_2O_3 phase causes continuous fluctuations in the friction coefficient. Coatings with high γ-Al_2O_3 content show significant differences in hardness and support force compared to pure aluminum, resulting in numerous groove defects and large fluctuations in the friction coefficient curve. Coatings with 60% aluminum content contain the most pure aluminum phase, exhibit the lowest porosity and hardness. High aluminum content leads to adhesive friction during operation. The pure aluminum phase envelops Al_2O_3 phases, causing aluminum adhesion to the grinding ball surface during friction. This forms an adhesive friction morphology, and repeated friction between the grinding ball causes Al_2O_3 phases to adhere and detach, leading to noticeable initial fluctuations in the friction coefficient.

Figure 8 presents wear data for coatings with varying aluminum content under a 10 N load for 30 min. The results show that pure AT3 specimens exhibited the least wear, while specimens containing 60% aluminum demonstrated the highest wear, significantly exceeding other groups. Error bars representing standard deviation (n = 3) are included in Figure 8. This discrepancy likely correlates with adhesive wear mechanisms [22,23]. As aluminum content increased, wear rates progressively rose, indicating that pure aluminum phase exhibits poor wear resistance. The addition of aluminum substantially reduces the coating's wear performance.

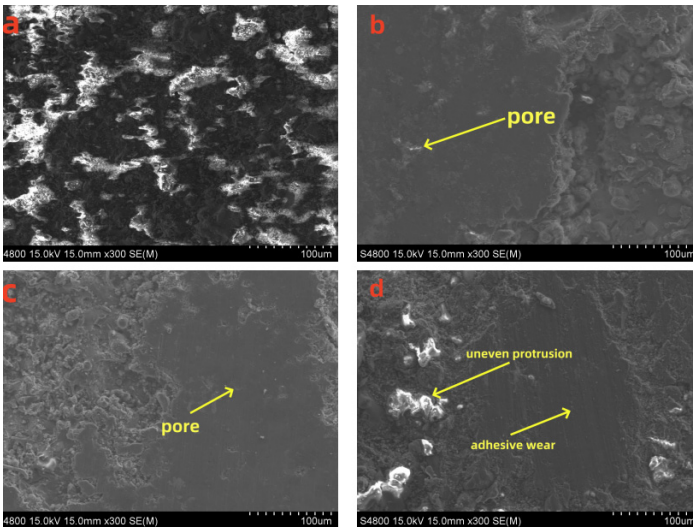

Figure 7. Scratch edge morphology of coatings with different Al contents (**a**): AT3-0% Al (**b**): AT3-20% Al (**c**): AT3-40% Al (**d**): AT3-60% Al.

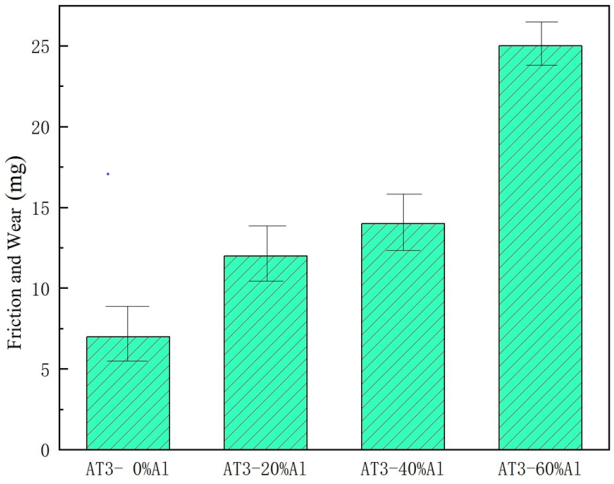

Figure 8. Wear of coatings with different Al contents.

3.5. Cross-Sectional Analysis of AT3 Coatings with Different Al Contents

Figure 9 shows the macroscopic morphology of the coating fracture. The pure AT3 coating fracture showed no impurity particles but exhibited elliptical pores and distinct cracks. These pores formed during the coating spraying process when molten droplets rapidly contracted, creating enclosed cavities that developed into elliptical voids during fracture propagation. Additionally, unmelted particles detached from the coating surface under external forces, also forming elliptical voids. The 20% aluminum content coating showed significantly fewer pores and no visible cracks, though minor pits at the fracture site likely resulted from partially melted particles. As aluminum content increased further, various particle types emerged in the coating: two primary forms were identified-non-conductive bright-side Al_2O_3 and dark-side pure aluminum phases. The bright-side particles markedly decreased at fracture surfaces, with both pore formation and crack probability being substantially reduced. Minor tear ridges appeared at fracture locations, particularly evident in 20% aluminum content coatings.

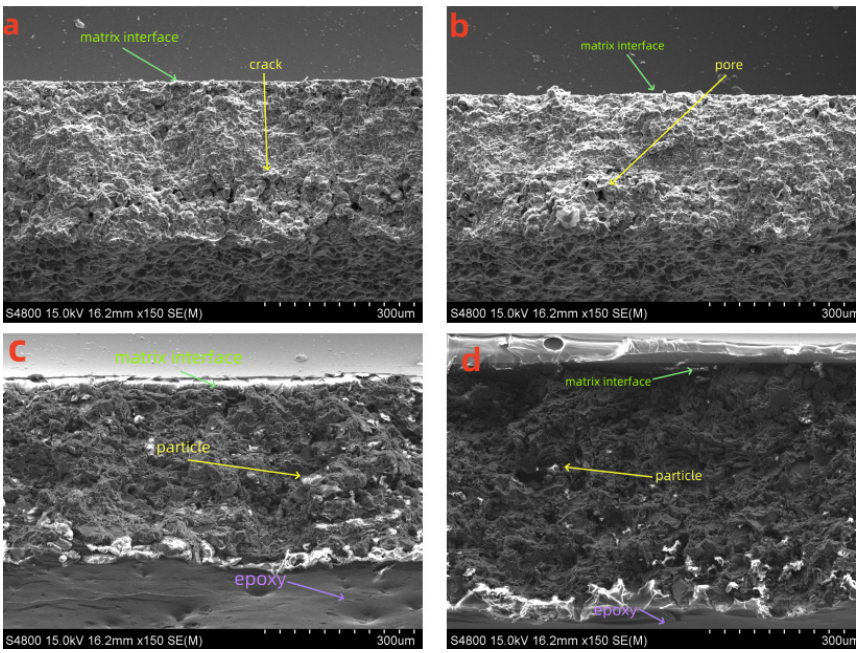

Figure 9. Morphology of coating fractures with different Al contents (**a**): AT3-0% Al (**b**): AT3-20% Al (**c**): AT3-40% Al (**d**): AT3-60% Al.

Figure 10 shows the high-magnification morphology of the fracture surface. The four coatings exhibit distinct trapezoidal, spherical, and irregular regions under high magnification. The AT3 coating demonstrates the largest trapezoidal area, containing stepped or spherical crystal planes formed by brittle fracture of its layered structure under mechanical stress. The prominent spherical regions originate from internal pores and coarse strip-like defects within the coating.

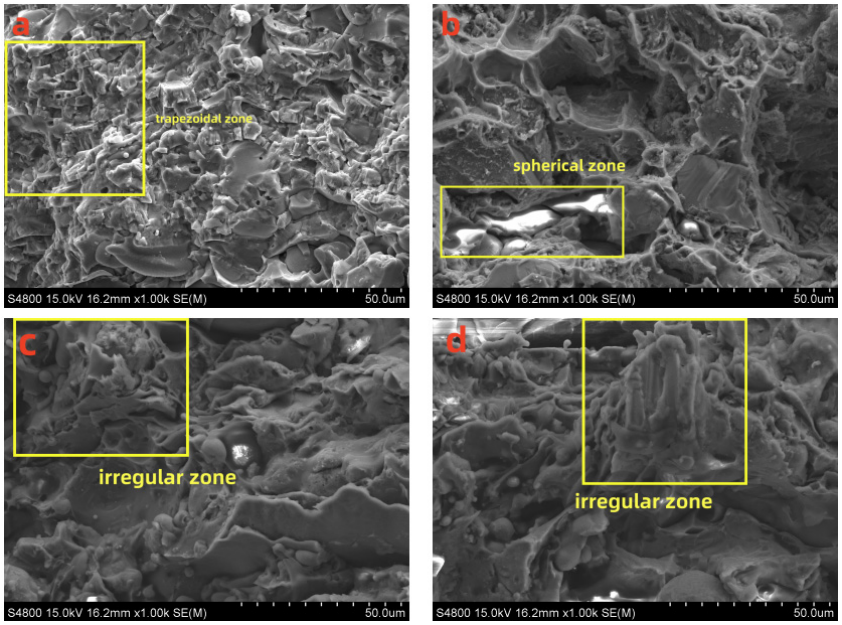

Figure 10. Morphology of coating fractures with different Al contents (**a**): AT3-0% Al (**b**): AT3-20% Al (**c**): AT3-40% Al (**d**): AT3-60% Al.

As the proportion of pure aluminum phase increases, the area of trapezoidal zones caused by brittle fracture formation decreases significantly. In coatings containing 60% aluminum content, trapezoidal zones become nearly undetectable. The spherical zone

at fracture surfaces gradually diminishes while irregular zones progressively expand. Therefore, incorporating pure aluminum phase can enhance coating toughness, mitigate excessive brittleness issues, and effectively prevent detachment or fracture during service.

4. Discussion

This study successfully fabricated AT3 composite coatings with varying aluminum content through plasma spraying and conducted a systematic investigation into the effects of pure aluminum phase incorporation on coating morphology, structure, and fundamental properties. Comprehensive evaluations were performed using surface morphology analysis, X-ray diffraction (XRD) analysis, porosity testing, tribological wear tests, and cross-sectional examination to assess the performance enhancement provided by pure aluminum compared to AT3 coatings. The key findings are summarized as follows:

(1) The incorporation of pure aluminum phases can alter the surface morphology of plasma spray AT3 coatings. The addition of aluminum phases induces wavy structures in the coating, which become more pronounced with increasing aluminum content. The cross-section exhibits elongated strip-like structures, reducing the occurrence of large pores and cracks. Simultaneously, the introduction of pure aluminum phases significantly promotes material phase transformation. The presence of pure aluminum phases reduces the intensity of α-Al_2O_3 diffraction peaks while continuously enhancing Al phase diffraction peaks. Due to the substantial melting point difference between pure aluminum and Al_2O_3, the γ-Al_2O_3 diffraction peaks at 40% aluminum content show a marked increase. XPS results demonstrate that the addition of pure aluminum phases introduces new pure aluminum peaks in the elemental spectrum, causing fluctuations in the original α-Al_2O_3 and γ-Al_2O_3 peaks. Additionally, the pore volume ratio of the coating first decreases, then increases, and subsequently declines again. The coating with 60% aluminum content exhibits the lowest porosity at 5.14% $\pm$ 0.52% at 60% Al content, which is lower than the 6.71% reported by Ren et al. [11] for 70% Al_2O_3 coatings.

(2) The addition of pure aluminum phases gradually reduces the coating's hardness. Simultaneously, fracture surfaces transition from brittle to irregular fractures, with the aluminum phase-induced cracks exhibiting irregular elongated patterns. This phase addition significantly improves the brittleness of AT3 coatings. Sliding friction wear tests demonstrate that the coating's coefficient of friction increases with higher aluminum content. The pure AT3 coating exhibits superior wear resistance due to its high hardness, showing no significant scratches during testing. While the 60% aluminum content achieves the highest friction coefficient and demonstrates the most severe frictional wear, surface adhesion wear occurs after reaching this level. This phenomenon correlates with the compositional phase structure and morphological characteristics of the aluminum-rich coating. The addition of pure aluminum phases gradually reduces the coating's hardness. This trade-off between toughness and wear resistance should be considered in industrial applications where both properties are critical.

Author Contributions: Writing—original draft, P.D.; Methodology, Y.Z.; Investigation, Software, X.W.; Validation, J.Y.; Resources, Writing—review & editing, L.Z.; Funding acquisition, X.Y. All authors have read and agreed to the published version of the manuscript.

Funding: This work was financially supported by the National Key Laboratory for Remanufacturing Fund "Preparation of Nickel based Metal Coatings with Multi Energy Field Coupling and Evaluation of High Temperature Oxidation Resistance", No. 61420052023KJW04.

Data Availability Statement: The original contributions presented in this study are included in the article. Further inquiries can be directed to the corresponding authors.

Conflicts of Interest: The authors declare no conflict of interest.

References

1. Wang, J.X.; Jiang, S.Q.; Pang, F.X. Current status and application of plasma spraying technology. *Mech. Manuf. Dig. (Weld. Sect.)* **2012**, *1*, 18–22.
2. Chen, L.M. Process, Microstructure and Properties of Plasma Spray Aluminum Oxide-Based Composite Ceramic Coatings. Ph.D. Thesis, Fuzhou University, Fuzhou, China, 2006.
3. Wang, W.Q. Study on the Microstructure and Properties of Plasma Spray Nano-Ceramic Thermal Barrier Coatings. Ph.D. Thesis, Jilin University, Changchun, China, 2005.
4. Zou, X.X. Research on Integrated Control Strategy and Application of Plasma Spray Multimodal Parameters. Master's Thesis, Hebei University of Science and Technology, Shijiazhuang, China, 2023.
5. Wu, D.; Liu, Y.; Zhao, X.; Li, D.; Ren, X. The tribological behaviors of different mass ratio Al_2O_3 TiO_2 coatings in water lubrication sliding against Si_3N_4. *J. Tribol. Trans.* **2016**, *59*, 352–362. [CrossRef]
6. Zhu, H.Q.; Liu, H.J.; Ding, M.H.; Zhang, C.; Liu, X.; Ming, L. Preparation and mechanical properties of low-pressure cold spray Cu-Ni-Al_2O_3 composite coatings. *Chem. Eng. New Mater.* **2024**, *52*, 187–191+206. [CrossRef]
7. Cao, B.W.; Li, H.J. Single point contour prediction of low-pressure cold spray aluminum coating. *China Surf. Eng.* **2025**, *38*, 338–349. [CrossRef]
8. Sun, Y.H.; Yan, H.; Lan, H.; Lan, H.; Huang, C.; Yu, S.; Sun, X.; Zhang, W. Study on the Microstructure and Corrosion Resistance of Laser-Cored Nickel-Al_2O_3 Composite Coatings. *Surf. Technol.* **2024**, *53*, 143–152.
9. Wang, Q.Q.; Li, S.N.; Cao, H.B.; Xu, K.; Tian, J. Effect of Al content on the microstructure and properties of plasma spray aluminum-Al_2O_3 composite coatings mimicking abalone shell structure. *J. Therm. Spray Technol.* **2024**, *16*, 84–99.
10. Wang, C.H.; Yang, C.L.; Wang, Y.H.; Li, X.; Zhao, J.; Gao, W.; Hao, G.; Wang, Y. Preparation of Al/Al_2O_3 Composite Spray Powder and Corrosion Resistance of Coatings. *J. Silic.* **2016**, *35*, 3759–3762+3769.
11. Ren, D.T.; Wang, W.Q.; Zhang, X.G.; Du, W.; Zhu, S. Study on the microstructure and corrosion resistance of magnesium alloy matrix supercritical plasma spray Al-Al_2O_3 composite coatings. *J. Mater. Her.* **2024**, *38*, 211–217.
12. Wang, K.; Cui, X.Y.; Wang, J.Q.; Xiong, T. Al_2O_3 Effect of particle content on the microstructure and mechanical properties of 7075Al/Al_2O_3 composite deposited layers by cold spray. *J. Therm. Spray Technol.* **2024**, *16*, 55–70. [CrossRef]
13. Fu, L.; Chen, X.M.; Liu, W. Performance of FeCrBSiNi wear-resistant coating prepared by supersonic arc spraying on Q235 steel surface. *J. Mech. Eng. Mater.* **2018**, *42*, 48–51. [CrossRef]
14. Sun, W.; Hong, S.; Wu, Y.P. Optimization of process parameters for WC-Cr_3C_2-Ni coating preparation by supersonic flame spraying. *J. Phys. Chem. Anal. (Phys. Sect.)* **2019**, *55*, 698–702+707. [CrossRef]
15. Zhao, D. Experimental Study on Surface Laser Cladding of Nano-Ceramic Coating on Titanium Alloy TC4. Master's Thesis, Nanjing University of Aeronautics and Astronautics, Nanjing, China, 2008.
16. Reimer, L. *Scanning Electron Microscopy: Physics of Image Formation and Microanalysis*; Springer: Berlin/Heidelberg, Germany, 1998.
17. Zhang, Y. Research on Key Technologies of Optical Glass Molding. Ph.D. Thesis, Tianjin University, Tianjin, China, 2020.
18. Micciulla, S.; Duan, X.; Strebe, J.; Löhmann, O.; Lamb, R.N.; von Klitzing, R. Transparent aluminiumoxide coatings of polymer brushes. *Angew. Chem. Int. Ed.* **2016**, *55*, 5028–5034. [CrossRef] [PubMed]
19. Ahmadvand, S.M.; Azarniya, A.; Hosseini, M.R.H. Thermomechanical synthesis of hybrid in-situ Al-(Al_3Ti+Al_2O_3) composites through nanoscale Al-Al_2TiO_5 reactive system. *J. Alloys Compd.* **2019**, *789*, 493–505. [CrossRef]
20. Irissou, E.; Legoux, J.G.; Arsenault, B.; Moreau, C. Investigation of Al-Al_2O_3 cold spray coating formation and properties. *J. Therm. Spray Technol.* **2007**, *16*, 661–668. [CrossRef]
21. Wang, C.; Chen, X.M.; Song, R.G. Effect of Nano-TiO_2 Content on Wear Resistance of Plasma Spray Al_2O_3/TiO_2 Coatings. *J. Met. Heat Treat.* **2018**, *43*, 192–196. [CrossRef]
22. Kong, R.; Liu, L.; Chen, Z.W. Adhesive wear analysis of hypoid gears under mixed-stream lubrication. *J. Mech. Transm.* **2025**, *49*, 105–113.
23. Liu, H.F.; Zhang, M.X.; Guo, C. Study on Friction and Wear of Mechanical Components. *J. Mod. Manuf. Technol. Equip.* **2024**, *60*, 22–24. [CrossRef]

Disclaimer/Publisher's Note: The statements, opinions and data contained in all publications are solely those of the individual author(s) and contributor(s) and not of MDPI and/or the editor(s). MDPI and/or the editor(s) disclaim responsibility for any injury to people or property resulting from any ideas, methods, instructions or products referred to in the content.